EUROPEAN ORGANIZATION FOR NUCLEAR RESEARCH

CERN-PPE/94-143
14 September 1994

B^* Production in Z Decays at LEP

The L3 Collaboration

Abstract

The production of B^* mesons in Z decays has been measured at LEP with the L3 detector. A sample of $Z \to b\bar{b}$ events was obtained by tagging muons in 1.6 million hadronic Z decays collected in 1991, 1992 and 1993. A signal with a peak value of $E_\gamma = 46.3 \pm 1.9$ (*stat*) MeV in the B rest frame energy spectrum was interpreted to come from the decay $B^* \to \gamma B$. The inclusive production ratio of B^* mesons relative to B mesons was determined from a fit to the spectrum to be

$$N_{B^*} \,/\, (N_{B^*} + N_B) = 0.76 \pm 0.08 \pm 0.06,$$

where the first error is statistical and the second is systematic.

(Submitted to Physics Letters B)

Introduction

Observation of the B^* meson was first reported by CUSB [1] and CLEO [2] in e^+e^- collisions at center-of-mass energies near the $\Upsilon(4S)$ resonance. Both experiments observed an excess of photons around 46 MeV and interpreted this as coming from the reaction $e^+e^- \to BB^*$, where $B^* \to \gamma B$. The mass splittings have been determined to be 46.0 ± 0.6 MeV [3] for B_d, B_u and 47.0 ± 2.6 MeV [1] for B_s. These values agree well with quark model predictions assuming the B^* to be the vector partner of the pseudoscalar B. As of yet, however, no direct measurement of the spin of the B^* has been made.

Hard fragmentation of the b quark in Z decays yields b hadrons with high momenta. Since photons produced in the decay $B^* \to \gamma B$ are boosted to energies up to 800 MeV, it is possible to directly detect the decay photon and to measure the relative production of B^* mesons to B mesons. This is performed at L3 by taking advantage of the excellent energy and angular resolution of its electromagnetic calorimetry. Note that here and throughout the paper B^* refers to the b-flavored *mesons* as a mixture of B_u^*, B_d^* and B_s^*; excited states of b-flavored *baryons* are expected to decay via pions or kaons to their ground states [4].

All B^* mesons are expected to decay to B mesons; so, a measurement of the production rate of B^* mesons in $Z \to b\bar{b}$ decays yields the ratio $N_{B^*} / (N_{B^*} + N_B)$ for a given b baryon fraction. If the B^* is assumed to be the vector partner of the pseudoscalar B meson, the relative production rate is a measurement of $V/(V+P)$, the fraction of vector meson production to the sum of vector and pseudoscalar meson production. This ratio may be estimated statistically from the number of degrees of freedom ($N_J = 2J+1$) of the two meson spin states ($J = 0, 1$) or at the individual quark level from Heavy Quark Effective Theory [5], assuming that orbital momentum and spin are decoupled. Both approaches exploit the fact that the b quark is heavy so that the vector and pseudoscalar states are nearly degenerate and predict $V/(V+P) \approx 0.75$.

There are at least two mechanisms, however, which may modify this prediction: the production of p-wave (B^{**}) mesons which subsequently decay to both B and B^* mesons and a spin-dependent fragmentation force [6] which influences both the production rate and the spin alignment of the B^*. Recent measurements of D^* production in $Z \to c\bar{c}$ decays at LEP have found $N_{D^*} / (N_{D^*} + N_D) \approx 0.5$ [7]. This relatively low rate of D^* production is not yet completely understood. A measurement of the relative production of B^* mesons to B mesons in $Z \to b\bar{b}$ decays provides a data point at higher quark mass.

The L3 Detector

The L3 detector is described in detail in reference 8. Central tracking is performed by a Time Expansion Chamber (TEC) consisting of two coaxial cylindrical drift chambers with 12 inner and 24 outer sectors [9]. A Z-chamber surrounding the TEC consists of two coaxial proportional chambers with cathode strip readout. The electromagnetic calorimeter is composed of bismuth germanate (BGO) crystals. Hadronic energy depositions are measured by a uranium-proportional wire chamber sampling calorimeter surrounding the BGO. Scintillator timing counters are located between the electromagnetic and hadronic calorimeters. The muon spectrometer, located outside the hadron calorimeter, comprises three layers of drift chambers measuring the muon trajectory in both the bending ($r - \phi$) and non-bending (z) planes. All subdetectors are installed inside a large magnet which provides a uniform field of 0.5 T.

The material preceding the central region of the BGO is less than 10% of a radiation length. In that region the energy resolution is 5% for photons and electrons of energies around 100 MeV and is better than 2% for energies above 1.5 GeV with a space angle resolution of approximately 3 mrad. Jets reconstructed from clusters in the electromagnetic and hadronic calorimeters have an angular resolution of approximately 2° and the total energy of hadronic events can be measured with a resolution of $\delta E / E = 10\%$ [10].

B^* Meson Selection

An inclusive selection of B^* mesons was performed by identifying the photon emitted in the decay $\mathrm{B}^* \to \gamma\mathrm{B}$. A sample of b-enriched events was obtained by tagging muons in semileptonic b hadron decays.[1)] Photon candidates were then selected from electromagnetic clusters located in the same hemisphere as the tagged muon jet. The B^* decay photons stand out as a peak above the background in the energy spectrum after a Lorentz transformation to the B meson rest frame. The B meson decay products were not explicitly reconstructed in this analysis. No distinction is made therefore between B_u^*, B_d^* and B_s^* since the mass splittings and production and decay kinematics for each of these excited meson states are approximately the same.

The analysis presented here is based on 1 587 774 hadronic Z decays collected in the years 1991, 1992 and 1993. These events satisfied both the online trigger and offline hadronic event selection criteria [11] with an efficiency of better than 99% and negligible contamination.

Muon tracks were reconstructed from segments in at least two of the three $r-\phi$ layers and at least one of the two z layers of the muon spectrometer. Each track was required to point toward the primary vertex in order to reduce background from hadronic punchthrough and cosmic rays coinciding with genuine hadronic events. The latter background was reduced to a negligible level by applying scintillator timing cuts.

The b-hadron content of the sample was enhanced by requiring each event to contain at least one muon candidate with momentum larger than 4 GeV and with momentum transverse to the closest hadronic jet larger than 1.2 GeV.

Each selected muon and its closest jet was tagged as a B meson decay candidate. The momentum of each candidate was then approximated in the following manner:

- The direction of the B momentum was determined from the vector sum of the muon momentum and the jet momentum.
- The magnitude of the B momentum was not estimated on an event by event basis, but was fixed to a common value, p_0. This method exploits the hard fragmentation of b quarks, which has been shown [12] to produce a sharply peaked momentum distribution.

Additional kinematic constraints were applied to the jets to reduce background and to improve the B momentum estimate: each jet was required to have an energy of at least 15 GeV and to be reconstructed from no more than 18 calorimetric clusters and no more than 10 TEC tracks. A total of 19 494 events satisfied these selection criteria.

The effect of the cuts on the B meson momentum distribution and angular resolution and the b purity of the sample were estimated by selecting Monte Carlo events in the same manner as data. More than 2.2 million hadronic Z decays were generated with Jetset 7.3 [13] and passed through the L3 detector simulation program [14]. Masses for the B and B^* mesons in the generator were set to the Particle Data Group [3] world averages.

The b purity of the selected event sample is estimated to be 84.2%, with 9% of these events fragmenting to b baryons and the rest to B mesons. The angular resolution for the B mesons is approximately 35 mrad. The value $p_0 = 37$ GeV was used as the approximate B meson momentum for all events. The spread around this value is estimated to be less than 20%.

Photon candidates were selected from reconstructed clusters located in the central BGO calorimeter ($|\cos\theta| < 0.69$) and in the same hemisphere of the event as the B meson. Each cluster was required to have a lateral shower shape consistent with an electromagnetic energy deposition. The cluster energy was determined from a matrix of nine crystals with the most energetic crystal being at the center. Each cluster was required to have a total energy of at least 100 MeV.

Background from non-electromagnetic processes was reduced and the energy resolution for photons was improved by requiring that the central crystal contain at least 50% and not more than 80% of the total energy of the cluster.

[1] A similar b hadron selection involving the tagging of electrons in semileptonic decays was studied. The electromagnetic cluster produced by the electron occupies a relatively large region of the BGO close to the jet axis. As a result, these events were found to be less suitable for the analysis than b decays involving muons.

Minimum ionizing particles tend to deposit a larger fraction of the energy in the central crystal and hadronic showers tend to be distributed more evenly over all nine crystals. Charged particle background was further reduced by requiring that there be no TEC tracks matching within a 60 mrad angle of the cluster at the radius of shower maximum. An isolation of 100 mrad in opening angle was required between the cluster and the selected muon.

The angle Φ_B, illustrated in Figure 1a, was defined as the angle between the selected muon track and the electromagnetic cluster in the plane perpendicular to the B meson direction. Distributions of data and Monte Carlo photon candidates in Φ_B are shown in Figure 1b. To reduce background from the hadronic side of the B decay, each cluster was required to satisfy $\cos\Phi_B > -0.7$. This cut rejects more than 35% of the background, while maintaining 85% of the signal photons.

The energy of each photon candidate in the approximate B rest frame was determined by performing the Lorentz transformation: $E_{\mathrm{rest}} = E_{\mathrm{lab}}\gamma(1-\beta\cos\alpha)$. Here, α is the angle between the photon direction and the B direction and γ and β are defined in terms of the approximate B meson momentum: $\gamma \equiv \sqrt{(p_0^2 + M_B^2)/M_B^2}$ and $\beta \equiv \sqrt{(\gamma^2-1)/\gamma^2}$. Since $M_{B^*} - M_B \ll M_B$, the recoil of the B is negligible and E_{rest} is a good approximation of the mass splitting.

Rest frame photon spectra are plotted in Figure 2 for data and Monte Carlo. The shaded region represents Monte Carlo clusters passing the photon selection but not coming from B^* photons. The B^* signal appears as an excess of photons around 50 MeV.

Results

A maximum likelihood fit was performed to the data rest frame photon spectrum allowing both signal and background parameters to float freely. The result is shown as the full line in Figure 3.

A bifurcated Gaussian was used to describe the signal region. This four-parameter function has the form

$$f(x) = \frac{2A}{(\sigma_1+\sigma_2)\sqrt{2\pi}} \times \begin{cases} e^{-(x-x_0)/2\sigma_1^2} & \text{for } x < x_0, \\ e^{-(x-x_0)/2\sigma_2^2} & \text{for } x \geq x_0. \end{cases}$$

where A is the total area, x_0 is the peak position, σ_1 is the width of the function below the peak and σ_2 is the width of the function above the peak.

The background was parametrized by performing a logarithmic transformation of the energy spectrum and then applying a fourth order Chebyshev polynomial expansion. This method, described in Reference 15, was chosen for its suitability to fit a distribution close to threshold. The advantage of this method is illustrated by the insert in Figure 3a, where the same fit is shown on a logarithmic energy scale.

The fit to the data spectrum yields a signal with a peak position at $E_\gamma = 46.3 \pm 1.9$ (*stat*) MeV. The number of B^* photons determined from the signal is

$$N_{B^*} = 1378 \pm 145\ (stat).$$

Uncertainty in the signal and background shapes contributes 119 events to this error.

The production rate was determined by comparing the number of B^* photons measured above with the number remaining in the Monte Carlo sample after applying the same selection. The Monte Carlo was normalized to the number of selected jets in the data. This procedure implicitly accounts for both the photon detection efficiency and the b purity.

The number of B^* mesons produced for each b hadron jet was determined from this method to be

$$N_{B^*} / N_{b-jet} = 0.69 \pm 0.07\ (stat).$$

The corresponding production ratio of B^* mesons to B mesons assuming a b-baryon fraction of $f_{\mathrm{baryon}} = 0.094$ is

$$N_{B^*} / (N_{B^*} + N_B) = 0.76 \pm 0.08\ (stat).$$

The method was checked by performing the same fitting procedure on the Monte Carlo energy spectrum including both signal and background. The peak of the signal was found from this fit to be $E_\gamma = 47.2 \pm 1.8$ MeV for an input mass splitting of $M_{B^*} - M_B = 46.0$ MeV. The number of B^* photons obtained from the fit is $N_{B^*} = 2316 \pm 289$ where the actual number of B^* photons in the Monte Carlo spectrum is $N_{B^*} = 2338$.

Contributions to the systematic uncertainty of the B^* production measurement are presented in Table 1. The fraction of b quarks fragmenting to b baryons was varied between 0.07 and 0.13. The b hadron purity was varied by $\pm$ 5% from the Monte Carlo estimate of 84.2% for the final event selection.

Source of Systematic Error	Error on $N_{B^*} / (N_{B^*} + N_B)$
b baryon fraction	0.02
b purity	0.03
b hadron selection	0.02
b fragmentation estimate	0.02
photon selection	0.05
Total	0.06

Table 1: *Systematic errors in the* $N_{B^*} / (N_{B^*} + N_B)$ *measurement.*

The effect of the b hadron selection on the fit result was further studied by varying the kinematic constraints on the jet, including energy and constituent multiplicity and the kinematic constraints on the selected muon, including momentum and transverse momentum to the jet. In addition, the average B meson momentum value, p_0, was varied between 35 GeV and 40 GeV.

Uncertainty in the B^* production ratio due to variations in the photon selection was estimated by systematically varying cut values while following the complete analysis chain for each selection combination. The B^* photon efficiency was determined from this procedure to vary by no more than 7%.

An additional study of the dependence of B^* photon efficiency on the selection was performed by measuring $\pi^0 \to \gamma\gamma$ signals in invariant mass spectra reconstructed from photon pairs in the selected events. One of the photons in each pair was required to satisfy the B^* photon cuts. The uncertainty of the B^* photon efficiency was checked by varying these cuts and comparing the π^0 rates for data and Monte Carlo.

The final systematic error was determined by adding in quadrature each of the individual uncertainties.

Conclusions

The relative production rate of B^* mesons to B mesons has been measured in $Z \to b\bar{b}$ decays at LEP. A b enriched sample of 19 494 events was selected by performing an inclusive muon tag on 1.6 million hadronic Z decays. The production ratio, determined from a maximum likelihood fit to the photon energy in the B rest frame, is

$$N_{B^*} / (N_{B^*} + N_B) = 0.76 \pm 0.08\ (stat) \pm 0.06\ (syst).$$

This ratio is an average measurement of $V / (V + P)$ for a mixture of the states B_d, B_u and B_s.

Acknowledgments

We wish to express our gratitude to the CERN accelerator divisions for the excellent performance of the LEP machine. We acknowledge the contributions of all the engineers and technicians who have participated in the construction and maintenance of this experiment.

The L3 Collaboration:

M.Acciarri[26], A.Adam[43], O.Adriani[16], M.Aguilar-Benitez[25], S.Ahlen[10], J.Alcaraz[17], A.Aloisio[28], G.Alverson[11], M.G.Alviggi[28], G.Ambrosi[33], Q.An[18], H.Anderhub[46], A.L.Anderson[15], V.P.Andreev[37], T.Angelescu[12], L.Antonov[40], D.Antreasyan[8], G.Alkhazov[37], P.Arce[25], A.Arefiev[27], T.Azemoon[3], T.Aziz[9], P.V.K.S.Baba[18], P.Bagnaia[36], J.A.Bakken[35], L.Baksay[42], R.C.Ball[3], S.Banerjee[9], K.Banicz[43], R.Barillère[17], L.Barone[36], A.Baschirotto[26], M.Basile[8], R.Battiston[33], A.Bay[19], F.Becattini[16], U.Becker[15], F.Behner[46], Gy.L.Bencze[13], J.Berdugo[25], P.Berges[15], B.Bertucci[33], B.L.Betev[40,46], M.Biasini[33], A.Biland[46], G.M.Bilei[33] R.Bizzarri[36], J.J.Blaising[4], G.J.Bobbink[17,2], R.Bock[1], A.Böhm[1], B.Borgia[36], A.Boucham[4], D.Bourilkov[46], M.Bourquin[19], D.Boutigny[17], B.Bouwens[2], E.Brambilla[15], J.G.Branson[38], V.Brigljevic[46], I.C.Brock[34], M.Brooks[23], A.Bujak[43], J.D.Burger[15], W.J.Burger[19], C.Burgos[25], J.Busenitz[42], A.Buytenhuijs[30], A.Bykov[37], X.D.Cai[18], M.Capell[15], G.Cara Romeo[8], M.Caria[33], G.Carlino[28], A.M.Cartacci[16], J.Casaus[25], R.Castello[26], N.Cavallo[28], M.Cerrada[25], F.Cesaroni[36], M.Chamizo[25], Y.H.Chang[48], U.K.Chaturvedi[18], M.Chemarin[24], A.Chen[48], C.Chen[6], G.Chen[6,46], G.M.Chen[6], H.F.Chen[20], H.S.Chen[6], M.Chen[15], G.Chiefari[28], C.Y.Chien[5], M.T.Choi[41], S.Chung[15], L.Cifarelli[8], F.Cindolo[8], C.Civinini[16], I.Clare[15], R.Clare[15], T.E.Coan[23], H.O.Cohn[31], G.Coignet[4], N.Colino[17], S.Costantini[36], F.Cotorobai[12], B.de la Cruz[25], X.T.Cui[18], X.Y.Cui[18], T.S.Dai[15], R.D'Alessandro[16], R.de Asmundis[28], A.Degré[4], K.Deiters[44], E.Dénes[13], P.Denes[35], F.DeNotaristefani[36], D.DiBitonto[42], M.Diemoz[36], H.R.Dimitrov[40], C.Dionisi[36], M.Dittmar[46], L.Djambazov[46], I.Dorne[4], M.T.Dova[18,♮], E.Drago[28], D.Duchesneau[19], F.Duhem[4], P.Duinker[2], I.Duran[39], S.Dutta[9], S.Easo[33], H.El Mamouni[24], A.Engler[34], F.J.Eppling[15], F.C.Erné[2], P.Extermann[19], R.Fabbretti[44], M.Fabre[44], S.Falciano[36], A.Favara[16], J.Fay[24], M.Felcini[46], T.Ferguson[34], D.Fernandez[25], G.Fernandez[25], F.Ferroni[36], H.Fesefeldt[1], E.Fiandrini[33], J.H.Field[19], F.Filthaut[30], P.H.Fisher[5], G.Forconi[15], L.Fredj[19], K.Freudenreich[46], M.Gailloud[22], Yu.Galaktionov[27,15], E.Gallo[16], S.N.Ganguli[9], P.Garcia-Abia[25], S.Gentile[36], J.Gerald[5], N.Gheordanescu[12], S.Giagu[36], S.Goldfarb[22], J.Goldstein[10], Z.F.Gong[20], E.Gonzalez[25], A.Gougas[5], D.Goujon[19], G.Gratta[32], M.W.Gruenewald[7], C.Gu[18], M.Guanziroli[18], V.K.Gupta[35], A.Gurtu[9], H.R.Gustafson[3], L.J.Gutay[43], A.Hasan[29], D.Hauschildt[2], J.T.He[6], T.Hebbeker[7], M.Hebert[38], A.Hervé[17], K.Hilgers[1], H.Hofer[46], H.Hoorani[19], S.R.Hou[48], G.Hu[18], B.Ille[24], M.M.Ilyas[18], V.Innocente[17], H.Janssen[4], B.N.Jin[6], L.W.Jones[3], P.de Jong[15], I.Josa-Mutuberria[17], A.Kasser[22], R.A.Khan[18], Yu.Kamyshkov[31], P.Kapinos[45], J.S.Kapustinsky[23], Y.Karyotakis[17], M.Kaur[18], S.Khokhar[18], M.N.Kienzle-Focacci[19], D.Kim[5], J.K.Kim[41], S.C.Kim[41], Y.G.Kim[41], W.W.Kinnison[23], A.Kirkby[32], D.Kirkby[32], S.Kirsch[45], W.Kittel[30], A.Klimentov[15,27], A.C.König[30], E.Koffeman[2], O.Kornadt[1], V.Koutsenko[15,27], A.Koulbardis[37], R.W.Kraemer[34], T.Kramer[15], V.R.Krastev[40,33], W.Krenz[1], H.Kuijten[30], K.S.Kumar[14], A.Kunin[15,27], P.Ladron de Guevara[25], G.Landi[16], D.Lanske[1], S.Lanzano[28,†], A.Lebedev[15], P.Lebrun[24], P.Lecomte[46], P.Lecoq[17], P.Le Coultre[46], D.M.Lee[23], J.S.Lee[41], K.Y.Lee[41], I.Leedom[11], C.Leggett[3], J.M.Le Goff[17], R.Leiste[45], M.Lenti[16], E.Leonardi[36], P.Levtchenko[37], C.Li[20,18], E.Lieb[45], W.T.Lin[48], F.L.Linde[2], B.Lindemann[1], L.Lista[28], Y.Liu[18], W.Lohmann[45], E.Longo[36], W.Lu[32], Y.S.Lu[6], J.M.Lubbers[17], K.Lübelsmeyer[1], C.Luci[36], D.Luckey[15], L.Ludovici[36], L.Luminari[36], W.Lustermann[44], W.G.Ma[20], M.MacDermott[46], M.Maity[9], L.Malgeri[36], R.Malik[18], A.Malinin[27], C.Maña[25], S.Mangla[9], M.Maolinbay[46], P.Marchesini[46], A.Marin[10], J.P.Martin[24], F.Marzano[36], G.G.G.Massaro[2], K.Mazumdar[9], P.McBride[14], T.McMahon[43], D.McNally[38], S.Mele[28], M.Merk[34], L.Merola[28], M.Meschini[16], W.J.Metzger[30], Y.Mi[22], A.Mihul[12], G.B.Mills[23], Y.Mir[18], G.Mirabelli[36], J.Mnich[1], M.Möller[1], V.Monaco[36], B.Monteleoni[16], R.Morand[4], S.Morganti[36], N.E.Moulai[18], R.Mount[32], S.Müller[1], E.Nagy[13], M.Napolitano[28], F.Nessi-Tedaldi[46], H.Newman[32], M.A.Niaz[18], A.Nippe[1], H.Nowak[45], G.Organtini[36], D.Pandoulas[1], S.Paoletti[36], P.Paolucci[28], G.Pascale[36], G.Passaleva[16,33], S.Patricelli[28], T.Paul[5], M.Pauluzzi[33], C.Paus[1], F.Pauss[46], Y.J.Pei[1], S.Pensotti[26], D.Perret-Gallix[4], A.Pevsner[5], D.Piccolo[28], M.Pieri[17], J.C.Pinto[34], P.A.Piroué[35], E.Pistolesi[16], F.Plasil[31], V.Plyaskin[27], M.Pohl[46], V.Pojidaev[27,16], H.Postema[15], N.Produit[19], J.M.Qian[3], K.N.Qureshi[18], R.Raghavan[9], G.Rahal-Callot[46], P.G.Rancoita[26], M.Rattaggi[26], G.Raven[2], P.Razis[29], K.Read[31], M.Redaelli[26], D.Ren[46], Z.Ren[18], M.Rescigno[36], S.Reucroft[11], A.Ricker[1], S.Riemann[45], B.C.Riemers[43], K.Riles[3], O.Rind[3], H.A.Rizvi[18], S.Ro[41], A.Robohm[46], F.J.Rodriguez[25], B.P.Roe[3], M.Röhner[1], S.Röhner[1], L.Romero[25], S.Rosier-Lees[4], R.Rosmalen[30], Ph.Rosselet[22], W.van Rossum[2], S.Roth[1], A.Rubbia[15], J.A.Rubio[17], H.Rykaczewski[46], J.Salicio[17], J.M.Salicio[25], E.Sanchez[25], G.S.Sanders[23], A.Santocchia[33], M.E.Sarakinos[43], S.Sarkar[9], G.Sartorelli[18], M.Sassowsky[1], G.Sauvage[4], C.Schäfer[1], V.Schegelsky[37], D.Schmitz[1], P.Schmitz[1], M.Schneegans[4], N.Scholz[46], H.Schopper[47], D.J.Schotanus[30], S.Shotkin[15], H.J.Schreiber[45], J.Shukla[34], R.Schulte[1], K.Schultze[1], J.Schwenke[1], G.Schwering[1], C.Sciacca[28], I.Scott[14], R.Sehgal[18], P.G.Seiler[44], J.C.Sens[17,2], L.Servoli[33], I.Sheer[38], S.Shevchenko[32], X.R.Shi[32], E.Shumilov[27], V.Shoutko[27], D.Son[41], A.Sopczak[17], V.Soulimov[28], C.Spartiotis[21], T.Spickermann[1], P.Spillantini[16], M.Steuer[15], D.P.Stickland[35], F.Sticozzi[15], H.Stone[35], K.Strauch[14], K.Sudhakar[9], G.Sultanov[18], L.Z.Sun[20,18], G.F.Susinno[19], H.Suter[46], J.D.Swain[18], A.A.Syed[30], X.W.Tang[6], L.Taylor[11], R.Timellini[8], Samuel C.C.Ting[15], S.M.Ting[15], O.Toker[33], M.Tonutti[1], S.C.Tonwar[9], J.Tóth[13], G.Trowitzsch[45], A.Tsaregorodtsev[37], G.Tsipolitis[34], C.Tully[35], J.Ulbricht[46], L.Urbán[13], U.Uwer[1], E.Valente[36], R.T.Van de Walle[30], I.Vetlitsky[27], G.Viertel[46], P.Vikas[18], U.Vikas[18], M.Vivargent[4], H.Vogel[34], H.Vogt[45], I.Vorobiev[14,27], A.A.Vorobyov[37], An.A.Vorobyov[37], L.Vuilleumier[22], M.Wadhwa[25], W.Wallraff[1], J.C.Wang[15], X.L.Wang[20], Y.F.Wang[15], Z.M.Wang[18,20], A.Weber[1], J.Weber[46], R.Weill[22], C.Willmott[25], F.Wittgenstein[17], D.Wright[35], S.X.Wu[18], S.Wynhoff[1], Z.Z.Xu[20], B.Z.Yang[20], C.G.Yang[6], G.Yang[18], X.Y.Yao[6], C.H.Ye[18], J.B.Ye[20], Q.Ye[18], S.C.Yeh[48], J.M.You[18], N.Yunus[18], M.Yzerman[2], C.Zaccardelli[32], P.Zemp[46], M.Zeng[18], Y.Zeng[1], D.H.Zhang[2], Z.P.Zhang[20,18], B.Zhou[10], G.J.Zhou[6], J.F.Zhou[1], R.Y.Zhu[32], A.Zichichi[8,17,18], B.C.C.van der Zwaan[2].

1 I. Physikalisches Institut, RWTH, D-52056 Aachen, FRG[§]
III. Physikalisches Institut, RWTH, D-52056 Aachen, FRG[§]
2 National Institute for High Energy Physics, NIKHEF, NL-1009 DB Amsterdam, The Netherlands
3 University of Michigan, Ann Arbor, MI 48109, USA
4 Laboratoire d'Annecy-le-Vieux de Physique des Particules, LAPP,IN2P3-CNRS, BP 110, F-74941 Annecy-le-Vieux CEDEX, France
5 Johns Hopkins University, Baltimore, MD 21218, USA
6 Institute of High Energy Physics, IHEP, 100039 Beijing, China
7 Humboldt University, D-10099 Berlin, FRG
8 INFN-Sezione di Bologna, I-40126 Bologna, Italy
9 Tata Institute of Fundamental Research, Bombay 400 005, India
10 Boston University, Boston, MA 02215, USA
11 Northeastern University, Boston, MA 02115, USA
12 Institute of Atomic Physics and University of Bucharest, R-76900 Bucharest, Romania
13 Central Research Institute for Physics of the Hungarian Academy of Sciences, H-1525 Budapest 114, Hungary[‡]
14 Harvard University, Cambridge, MA 02139, USA
15 Massachusetts Institute of Technology, Cambridge, MA 02139, USA
16 INFN Sezione di Firenze and University of Florence, I-50125 Florence, Italy
17 European Laboratory for Particle Physics, CERN, CH-1211 Geneva 23, Switzerland
18 World Laboratory, FBLJA Project, CH-1211 Geneva 23, Switzerland
19 University of Geneva, CH-1211 Geneva 4, Switzerland
20 Chinese University of Science and Technology, USTC, Hefei, Anhui 230 029, China
21 SEFT, Research Institute for High Energy Physics, P.O. Box 9, SF-00014 Helsinki, Finland
22 University of Lausanne, CH-1015 Lausanne, Switzerland
23 Los Alamos National Laboratory, Los Alamos, NM 87544, USA
24 Institut de Physique Nucléaire de Lyon, IN2P3-CNRS,Université Claude Bernard, F-69622 Villeurbanne Cedex, France
25 Centro de Investigaciones Energeticas, Medioambientales y Tecnologicas, CIEMAT, E-28040 Madrid, Spain
26 INFN-Sezione di Milano, I-20133 Milan, Italy
27 Institute of Theoretical and Experimental Physics, ITEP, Moscow, Russia
28 INFN-Sezione di Napoli and University of Naples, I-80125 Naples, Italy
29 Department of Natural Sciences, University of Cyprus, Nicosia, Cyprus
30 University of Nymegen and NIKHEF, NL-6525 ED Nymegen, The Netherlands
31 Oak Ridge National Laboratory, Oak Ridge, TN 37831, USA
32 California Institute of Technology, Pasadena, CA 91125, USA
33 INFN-Sezione di Perugia and Universitá Degli Studi di Perugia, I-06100 Perugia, Italy
34 Carnegie Mellon University, Pittsburgh, PA 15213, USA
35 Princeton University, Princeton, NJ 08544, USA
36 INFN-Sezione di Roma and University of Rome, "La Sapienza", I-00185 Rome, Italy
37 Nuclear Physics Institute, St. Petersburg, Russia
38 University of California, San Diego, CA 92093, USA
39 Dept. de Fisica de Particulas Elementales, Univ. de Santiago, E-15706 Santiago de Compostela, Spain
40 Bulgarian Academy of Sciences, Institute of Mechatronics, BU-1113 Sofia, Bulgaria
41 Center for High Energy Physics, Korea Advanced Inst. of Sciences and Technology, 305-701 Taejon, Republic of Korea
42 University of Alabama, Tuscaloosa, AL 35486, USA
43 Purdue University, West Lafayette, IN 47907, USA
44 Paul Scherrer Institut, PSI, CH-5232 Villigen, Switzerland
45 DESY-Institut für Hochenergiephysik, D-15738 Zeuthen, FRG
46 Eidgenössische Technische Hochschule, ETH Zürich, CH-8093 Zürich, Switzerland
47 University of Hamburg, 22761 Hamburg, FRG
48 High Energy Physics Group, Taiwan, China
§ Supported by the German Bundesministerium für Forschung und Technologie
‡ Supported by the Hungarian OTKA fund under contract number 2970.
♯ Also supported by CONICET and Universidad Nacional de La Plata, CC 67, 1900 La Plata, Argentina
† Deceased.

References

[1] CUSB Collaboration J. Lee-Franzini *et al.*, Phys. Rev. Lett. **65** (1990) 2947;
K. Han *et al.*, Phys. Rev. Lett. **55** (1985) 36.

[2] CLEO Collaboration D.S. Akerib *et al.*, Phys. Rev. Lett. **67** (1991) 1692.

[3] Particle Data Group, Phys. Rev. **D45** (1992).

[4] W. Kwong, J.L. Rosner, C. Quigg, Ann. Rev. Nucl. Part. Sci. **37** (1987) 325.

[5] A. Falk and M. Peskin, Phys. Rev. **D49** (1994) 3320.

[6] M. Suzuki, Phys. Rev. **D33** (1986) 676.

[7] DELPHI Collaboration, P. Abreu *et al.*, Z Phys. **C59** (1993) 533.

[8] L3 Collaboration, B. Adeva *et al.*, Nucl. Instr. and Meth. **A289** (1990) 35.

[9] F. Beissel *et al.*, Nucl. Instr. and Meth. **A332** (1993) 33.

[10] O. Adriani *et al.*, Nucl. Instr. and Meth. **A302** (1991) 53.

[11] L3 Collaboration, B. Adeva *et al.*, Z. Phys. **C51** (1991) 179.

[12] L3 Collaboration, B. Adeva *et al.*, Phys. Lett. **B261** (1991) 177.

[13] T. Sjöstrand, Comp. Phys. Comm. **39** (1986) 347;
T. Sjöstrand and M. Bengtsson, Comp. Phys. Comm. **43** (1987) 367.

[14] The L3 detector simulation program is based on the GEANT program:
R. Brun *et al.*, "GEANT 3", CERN report **DD/EE/84-1** (1984) (Revised), September 1987.
Hadronic interactions in the detector were modelled with GHEISHA:
H. Fesefeldt, RWTH Aachen report **PITHA 85/02** (1985).
Events were corrected for the TEC, BGO and muon chamber inefficiencies obtained from the data.

[15] Numerical Approximations to Functions and Data,
Chapter 5: Curve Fitting by Polynomials in One Variable
J.G. Hayes, University of London, The Athlone Press (1970).

Figure Captions

Figure 1. a) Schematic diagram of the Φ_B cut. This cut decreases background from the hadronic recoil of the B decay.
b) Distribution of Φ_B for data and Monte Carlo photon candidates. The region between the two arrows was excluded.

Figure 2. Data and Monte Carlo rest frame photon energy spectra.

Figure 3. a) Likelihood fit to the data rest frame photon energy spectrum.
b) B^* signal after subtraction of fit to background.

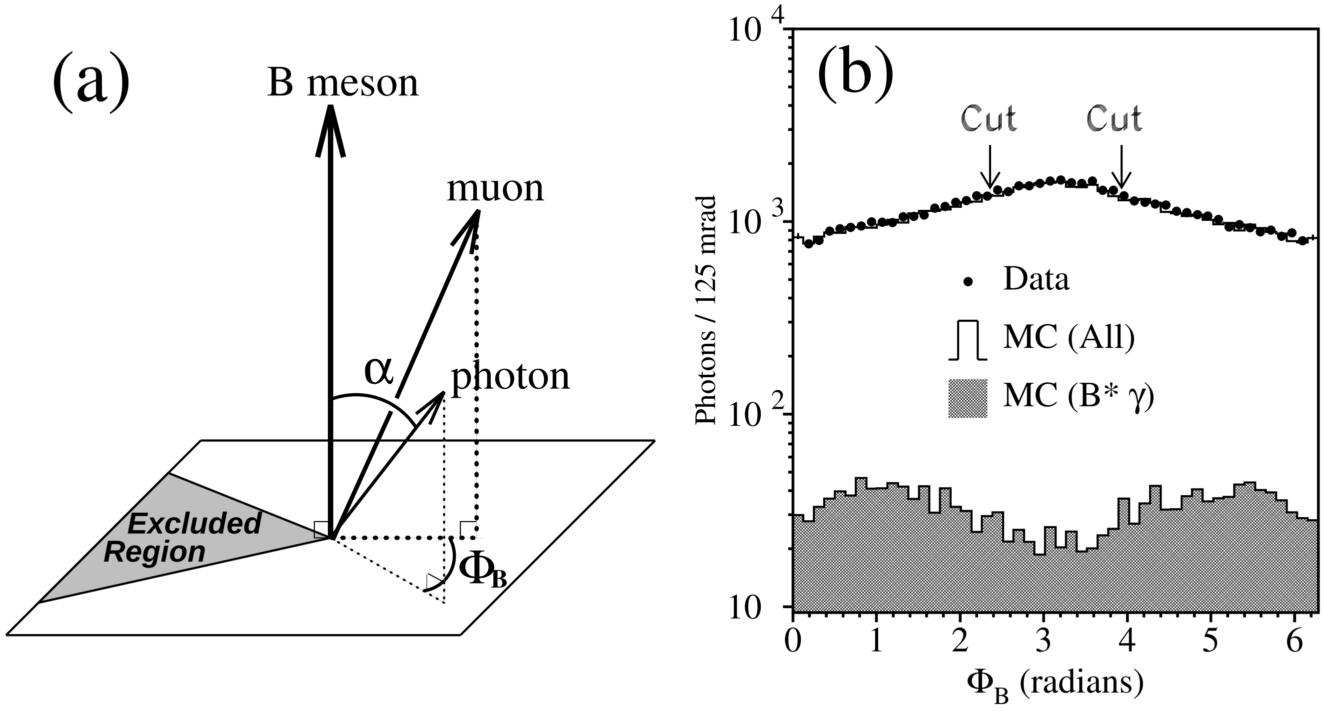

(a)
B meson
muon
photon
α
Excluded Region
Φ_B
(b)
Cut
Cut
Data
MC (All)
MC (B* γ)
Photons / 125 mrad
Φ_B (radians)

Figure 1

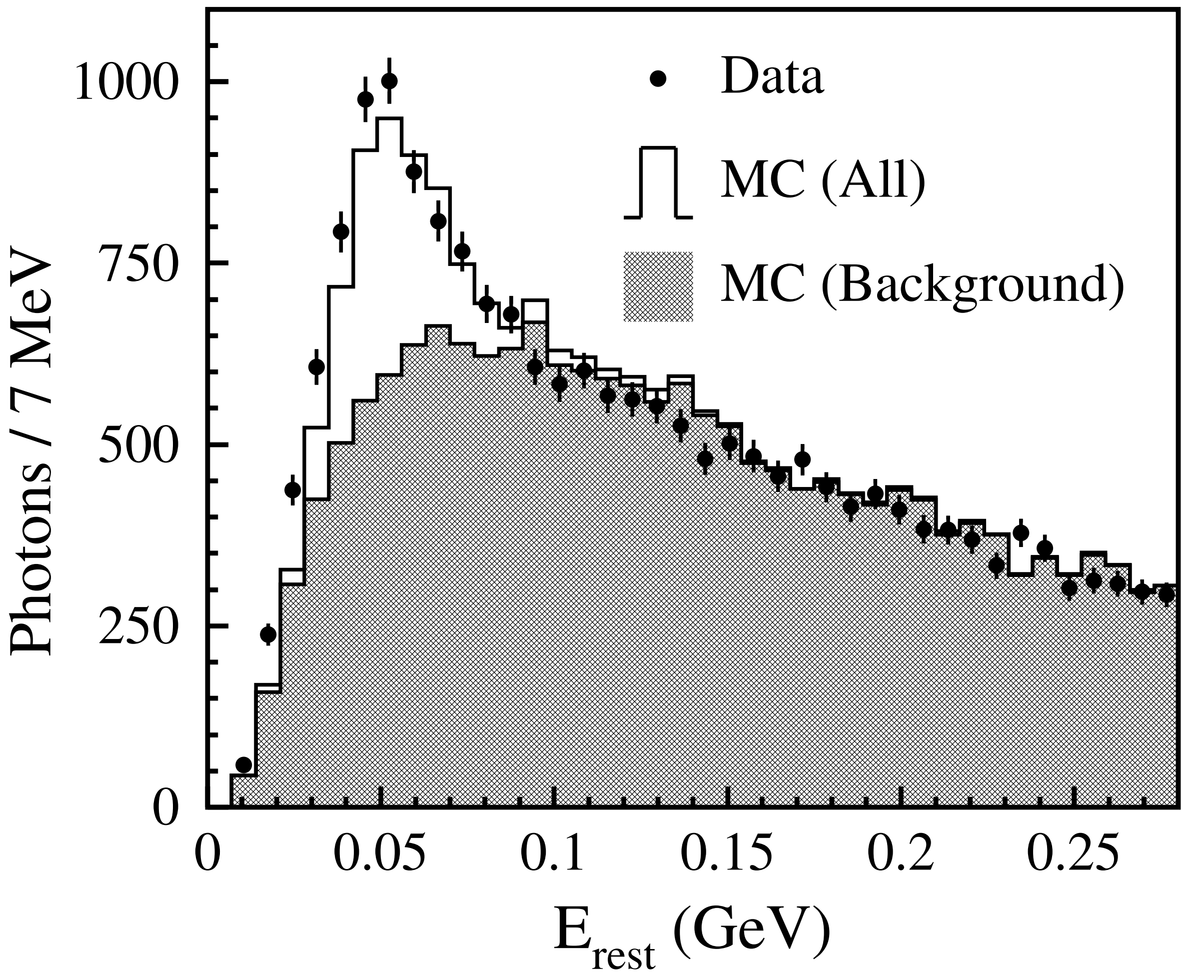

Data
MC (All)
MC (Background)
Photons / 7 MeV
1000
750
500
250
0
0
0.05
0.1
0.15
0.2
0.25
E_rest (GeV)

Figure 2

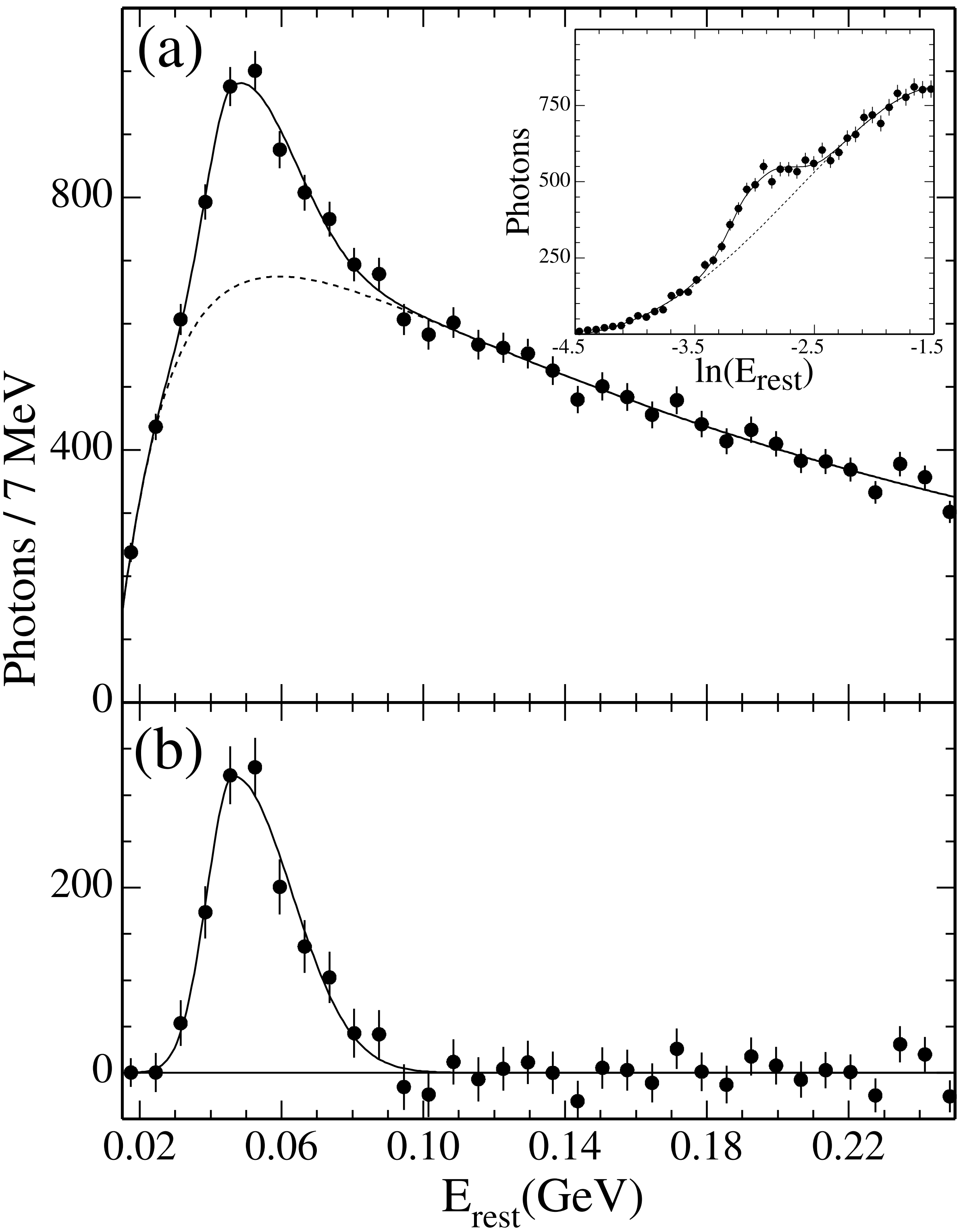

(a)
(b)
Photons / 7 MeV
800
400
0
200
0
0.02
0.06
0.10
0.14
0.18
0.22
E_{rest}(GeV)
Photons
750
500
250
-4.5
-3.5
-2.5
-1.5
ln(E_{rest})

Figure 3